

pubs.acs.org/macroletters Letter

Asymmetric Molecular Dynamics and Anisotropic Phase Separation in the Cocrystal of the Crystalline/Crystalline Polymer Blend

Ying Zheng,[#] Navin Kafle,[#] Derek Schwarz, James M. Eagan, Shigetaka Hayano, Yuki Nakama,* Pengju Pan,* and Toshikazu Miyoshi*



Cite This: ACS Macro Lett. 2022, 11, 193–198



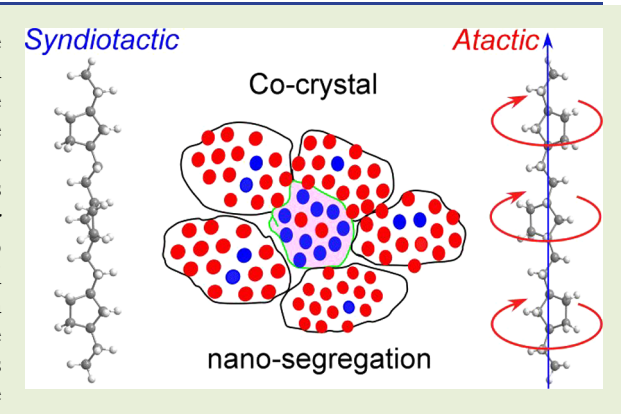
ACCESS

III Metrics & More



SI Supporting Information

ABSTRACT: Semicrystalline polymers are categorized as either mobile or fixed crystals, depending on chain mobility in the crystalline region. In this work, we investigate molecular dynamics and phase structure in the cocrystal consisting of fixed and mobile polymer crystals by solid-state (ss) nuclear magnetic resonance (NMR) spectroscopy. It is demonstrated that (i) the mobile component begins large amplitude motions associated with crystal—crystal transition, while fixed ones keep their rigidity in the cocrystal, and (ii) asymmetric molecular dynamics leads to nanosegregations into mobile- and fixed-rich domains in the cocrystal below the melting temperature $(T_{\rm m})$. The observed phase separation induced by asymmetric molecular dynamics is similar to the phase separation of the miscible amorphous polymer blend; however, it is limited to two dimensions due to the parallel packing of the stems inside the cocrystal, as well as chain connectivity at the crystalline—amorphous boundary.



olecular dynamics of polymer chains in the crystalline region of semicrystalline polymers is a crucial factor for crystallinity, $^{1-7}$ lamellar thickness, $^{1-7}$ deformability, 8,9 and mechanical properties. Flexible semicrystalline polymers, such as polyethylene, 12,13 isotactic (i)-polypropylene, 14 poly(ethylene oxide), 15 poly(tetrafluoro ethylene), 16 and so on, experience large amplitude molecular motions in the crystalline region, including anisotropic rotations around the chain axis, which are concomitant with translations along the chain axis (mobile crystals), whereas poly(ethylene terephthalate) (PET), 17 Nylon, 18 syndiotactic (s)-PP, 8 i-poly(1-butene) form I, and so on do not conduct chain dynamics up to the melting temperature ($T_{\rm m}$; fixed crystals). Mobile crystals show much higher crystallinity, $^{1-7}$ longer lamellae thickness, $^{1-7}$ higher molecular orientation, 19 and resultantly higher mechanical properties after processing 10,11 than those for fixed crystals.

A polymer blend is an attractive and conventional approach to alter polymer structure, dynamics, and properties. 20 In miscible blends, various polymer mixtures show a single glass transition temperature $(T_{\rm g})$ that is different from $T_{\rm gs}$ for individual components A and B $(T_{\rm gA}$ and $T_{\rm gB}).^{21}$ By applying various experimental techniques, it was reported that individual components possess inherent dynamic behaviors (asymmetric molecular dynamics) even in the miscible blends. $^{22-24}$ Asymmetric molecular dynamics leads to isotropic phase separations above the lower critical solution temperature (LCST). 25,26 Previous studies have been conducted on

miscible amorphous polymer blends^{21–26} but not crystalline/crystalline ones, because most semicrystalline polymers do not cocrystallize. If mobile and fixed polymer crystals cocrystallize together, how does cocrystallization alter molecular dynamics, crystalline structure, and mechanical and thermal properties in the blend?

In recent years, novel polyolefins, stereoregular hydrogenated polynorbornene (hPNB)s, 27 in addition to an existing stereoirregular one, 27,28 were successfully synthesized via stereoselective ring-opening polymerization. Interestingly, all s-, i-, and atactic (a)-hPNBs crystallize in monoclinic (a = 5.97 Å, b = 9.48 Å, c = 12.58 Å, and β = 60°), orthorhombic (a = 5.95 Å, b = 8.25 Å, c = 12.65 Å), and monoclinic lattices (a = 5.43 Å, b = 9.45 Å, c = 12.41 Å, and β = 90°), respectively, where all three adopt a nearly trans-conformation (c = 12.41–12.65 Å) independent of stereoregularity. 29 Moreover, Kafle et al. reported that (i) s- and i-hPNBs are fixed crystals, while a-hPNB conducts large amplitude motions associated with a crystal—crystal transition into the rotator phase (mobile crystal) at T_{cc} = 115 °C, and (ii) a-hPNB shows a much

Received: November 28, 2021 Accepted: January 12, 2022 Published: January 14, 2022





higher crystallinity (Φ_c = 82%) and a much longer long period (L = 80 nm) than those for stereoregular ones (Φ_c = 50–55% and L = 17–21 nm). These unique structures for the configurationally disordered crystal are attributed to very fast molecular dynamics in the high-temperature phase.

In this work, we for the first time investigate cocrystallization, molecular dynamics, and microscopic phase structure for the a-/s-hPNB blend at high temperatures above $T_{\rm cc}$ by using differential scanning calorimetry (DSC) and ssNMR spectroscopy. The asymmetric a-/s-hPNB blend with a mixing ratio of 3:1, respectively, was prepared by solution blending. Detailed experimental conditions, including sample preparation, DSC, and ssNMR experiments, are provided in the Supporting Information (SI).

Figure 1 shows DSC thermographs for pure *a*- and *s*-hPNBs and their blend with cooling and heating rates of 10 °C/min. *a*-

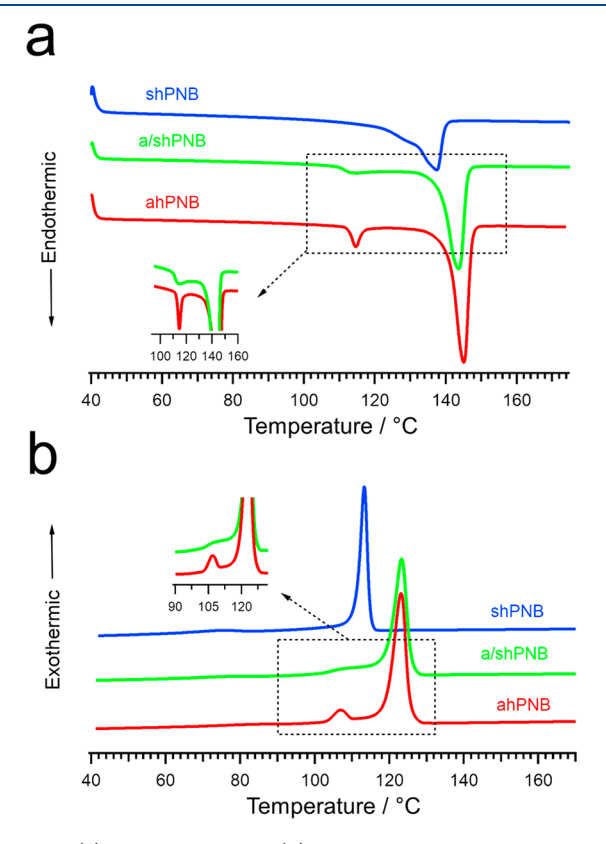


Figure 1. (a) DSC heating and (b) cooling thermographs for pure a-and s-hPNBs and their blend with heating and cooling rates of 10 $^{\circ}$ C/min.

hPNB experiences a crystal—crystal transition at 115 and 108 °C during heating and cooling, respectively, while s-hPNB does not. The blend, very broad crystal—crystal transition peaks are observed at 110–125 and 100–115 °C during heating and cooling, respectively. $T_{\rm m}$ and crystallization temperature ($T_{\rm c}$) for the blend are 145 and 122 °C, respectively, which are similar to those for a-hPNB, but $T_{\rm m}$ and $T_{\rm c}$ corresponding to pure s-hPNB are not observed in the blend. These thermal behaviors indicate cocrystallization of a- and s-hPNBs in the blend.

¹³C CPMAS NMR spectra for pure samples and the blend and signal assignment are depicted in Figure S1. Figure 2a shows an expanded ¹³C CPMAS NMR spectrum for the C7 and C1,4 signals for the blend measured at 123 °C. The C7

signal at 44.2 ppm is attributed to the overlapped *a*- and *s*-hPNB crystalline signals, while the C1,4 signal shows different chemical shift values for *a*- (43.4 ppm) and *s*-hPNB (42.0 ppm) crystalline signals and overlapped amorphous signals (41.6 ppm) in the blend.⁷

Figure 2b shows chemical shift anisotropy (CSA) spectra for the C7 carbon for pure a- (red) and s-hPNBs (blue) at 123 °C and their conformations with orientations of the CSA principal axes. The CSA spectrum for s-hPNB shows an axially asymmetric pattern that is similar to that for a-hPNB at 25 °C reported in previous work,7 where crystalline stem dynamics is frozen. The spectral pattern was reproduced by the calculated CSA pattern (blue dashed line) with principal values, $(\sigma_{11}, \sigma_{22}, \sigma_{33}) = (64, 45, 23 \text{ ppm})$. Moreover, a onedimensional exchange NMR indicated that there is no slow chain dynamics in the s-hPNB crystalline region $(10^{-2}-10^2 \text{ s})$ up to $T_{\rm m}$. These results indicate that large amplitude motions are frozen in the s-hPNB crystal even at 123 °C, just below $T_{\rm m}$ = 137 °C (Figure 2b). On the other hand, the a-hPNB crystalline signal shows an axially symmetric pattern with $(\sigma_{11},$ σ_{22} , σ_{33}) = (55, 55, 23 ppm) at 123 °C. Under the assumption of uniaxial rotation around the σ_{33} axis (chain axis) in a frequency over 20 kHz (Figure 2b), the simulated curve (red dashed line) could reproduce the experimental one. The CSA pattern for the C7 signal in the cocrystal (green solid line in Figure 2c) shows an axially symmetric pattern that is almost the same as that for pure a-hPNB. This means that major stems participate in the large amplitude motions in the cocrystal. Summations (green dashed) of stoichiometryweighted axially symmetric (red dashed) and asymmetric (blue dashed) patterns are well consistent with the experimental one (Figure 2c). However, it may be challenging to properly characterize chain dynamics for the minor s-hPNB stems in the cocrystal via the CSA line-shape analysis for the overlapped signals. The C1,4 CSA patterns for pure s- (blue solid line) and a-hPNBs (red) and their cocrystal (green) are depicted in Figure 2d,e. As expected, the C1,4 CSA pattern for a-hPNB in the cocrystal shows the same axially symmetric pattern with that for pure a-hPNB (Figure 2e). On the other hand, pure s-hPNB shows invariant asymmetric patterns at 25 °C (bottom blue in Figure 2d) and 123 °C (middle blue in Figure 2d). The C1,4 CSA pattern for s-hPNB in the cocrystal depicts the same pattern with those for pure s-hPNB. This result indicates that most s-hPNB stems do not conduct large amplitude motions in the cocrystal at 123 °C. It is concluded that two components conduct largely different chain dynamics (asymmetric chain dynamics) in the cocrystal above T_{cc} .

¹³C spin-lattice relaxation time in the laboratory frame (T_{1C}) is a conventional tool to capture small amplitude motions in the range of the ¹³C Larmor frequency of 75 MHz, which is larger by three orders of magnitude than the dynamics range detected by CSA. The conventional experiment has been successfully used in the analysis of molecular dynamics of a polymer in solution and melt states.³² The C1,4 signal for pure s-hPNB in the crystalline region (blue open circles) possesses T_{1C} values of about 328.9 s at 100 °C and 291.6 s at 130 °C, respectively (Figure 3a,b). On the other hand, pure a-hPNB shows quite short T_{1C} values of 1.7 s (red open circles) at 100 $^{\circ}$ C (below T_{cc}) and 2.3 s at 130 $^{\circ}$ C (above T_{cc}). These values are very close to those in the amorphous region (e.g., 0.67 s at 130 °C, see details in Table S1). This fact indicates that small amplitude motions are well activated in the a-hPNB crystalline region, even below T_{cc} . Configurational disorder makes some

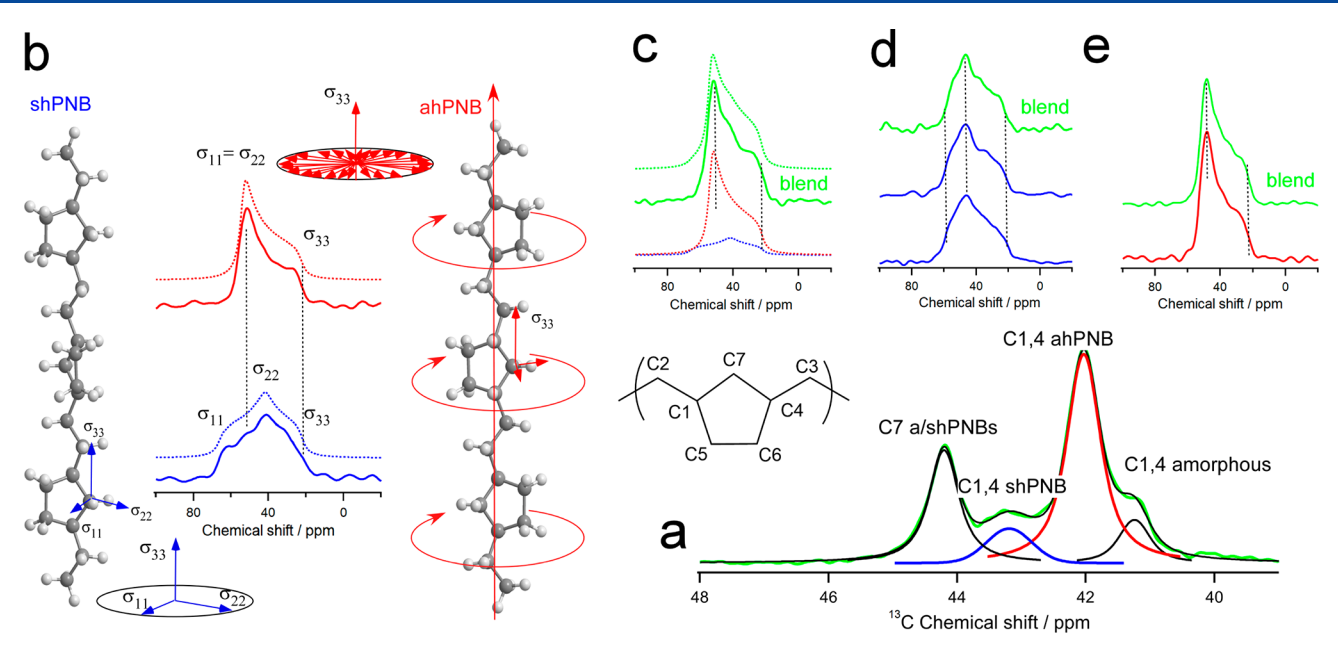


Figure 2. (a) ¹³C CPMAS NMR spectrum for the *a-/s*-hPNB blend with a mixing ratio of 3:1, respectively, in the chemical shift range of 39–48 ppm at 123 °C. ¹³C CSA spectra for (b, c) C7 and (d, e) C1,4 signals for pure *a-* (red) and *s*-hPNBs (blue) and their blend (green) measured by using SUPER³⁰ at 25 and 123 °C and (b, c) simulated CSA patterns (dashed lines) for pure *a-* (red) and *s*-hPNBs (blue) and the blend (green). (b) Chain conformation for pure *a-* and *s*-hPNBs determined in ref 29 and their dynamic models with orientations for the CSA principle axes on the C7 carbon.⁷

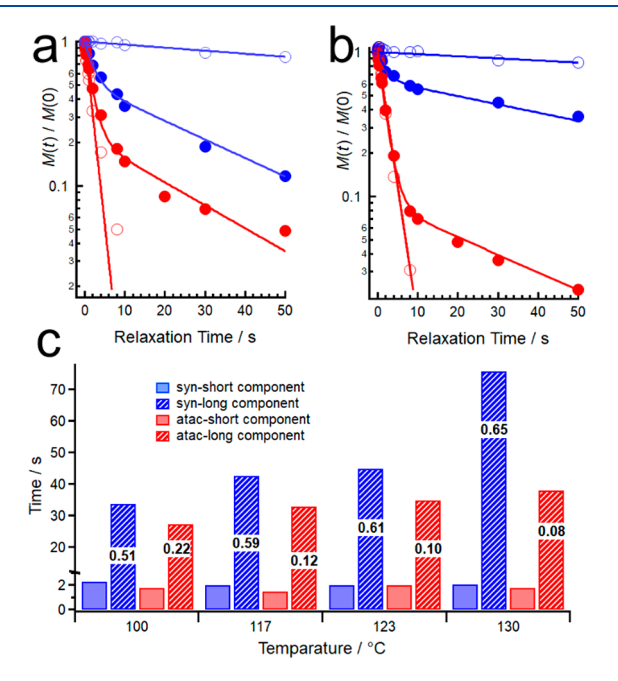


Figure 3. $T_{\rm 1C}$ relaxation decays for pure *a*- and *s*-hPNBs and their cocrystal at (a) 100 and (b) 130 °C. (c) $T_{\rm 1C}$ values for *a*- and *s*-hPNBs in the cocrystal and the relative fraction for the long component.

dynamics spaces for librations in the crystalline region. A large variation in the $T_{\rm 1C}$ values between a- and s-hPNBs may be useful to study the cocrystallization effect on the small amplitude motions for two components.

At 100 °C, both a- (red filled circles) and s-hPNBs (blue) obviously show double exponential decays in the cocrystal, which are largely different from those in pure samples. This indicates that small amplitude motions in the stems are significantly affected by cocrystallization. Above T_{cc} separa-

tions in the relaxation curves between a- and s-hPNBs are prominent at 117 °C (Figure S2a). With further increasing temperature, separation gets larger and larger (Figures S2b and 3b). All relaxation curves in the cocrystal were analyzed in terms of double exponential curves. The relaxation values and their fractions for a- and s-hPNBs in the cocrystal are plotted in Figure 3c and are listed in Table S1. The short T_{1C} values for a-hPNB in the cocrystal at all the temperatures are similar to those for pure a-hPNB. Their fractions increase with increasing temperature. Interestingly, s-hPNB in the cocrystal also shows very similar short T_{1C} values of 1.9-2.3 s with those for ahPNB. This means that small amplitude motions in minor shPNB stems in the cocrystal are significantly enhanced by major mobile a-hPNB stems. Surprisingly, the T_{1C} values for the long components of a- and s-hPNBs in the cocrystal increase with increasing temperature. In general, solid polymer dynamics is thermally activated and leads to a shorter T_{1C} value with increasing temperature.³² The observed opposite trend suggests slowing down molecular dynamics with increasing temperature. Moreover, a relative fraction for the long component decreases in a-hPNB, while it increases in shPNB in the cocrystal. The observed temperature dependence of the dynamic heterogeneity in the cocrystal suggests phase separations into a- and s-hPNB-rich domains in the cocrystal with increasing temperature above T_{cc} .

To investigate spatial heterogeneity of a- and s-hPNB stems in the cocrystal, ${}^{1}H$ spin—lattice relaxation time in the rotating frame $(T_{1\rho H})$, which has been successfully utilized to characterize miscibility as well as phase separation of polymer blends at several nm scales, 31,32 was measured. Figure 4a,b shows $T_{1\rho H}$ decaying curves for pure a- (red open circles) and s-hPNBs (blue) and their blend (filled circles) at 100 and 130 ${}^{\circ}C$, respectively. Pure a- and s-hPNBs show single $T_{1\rho H}$ values of 15.4 and 71.4 ms, respectively, at 100 ${}^{\circ}C$. With increasing the temperature above T_{co} pure a-hPNB stems begin fast chain dynamics over 20 kHz and thus lead to a large reduction to 6.6

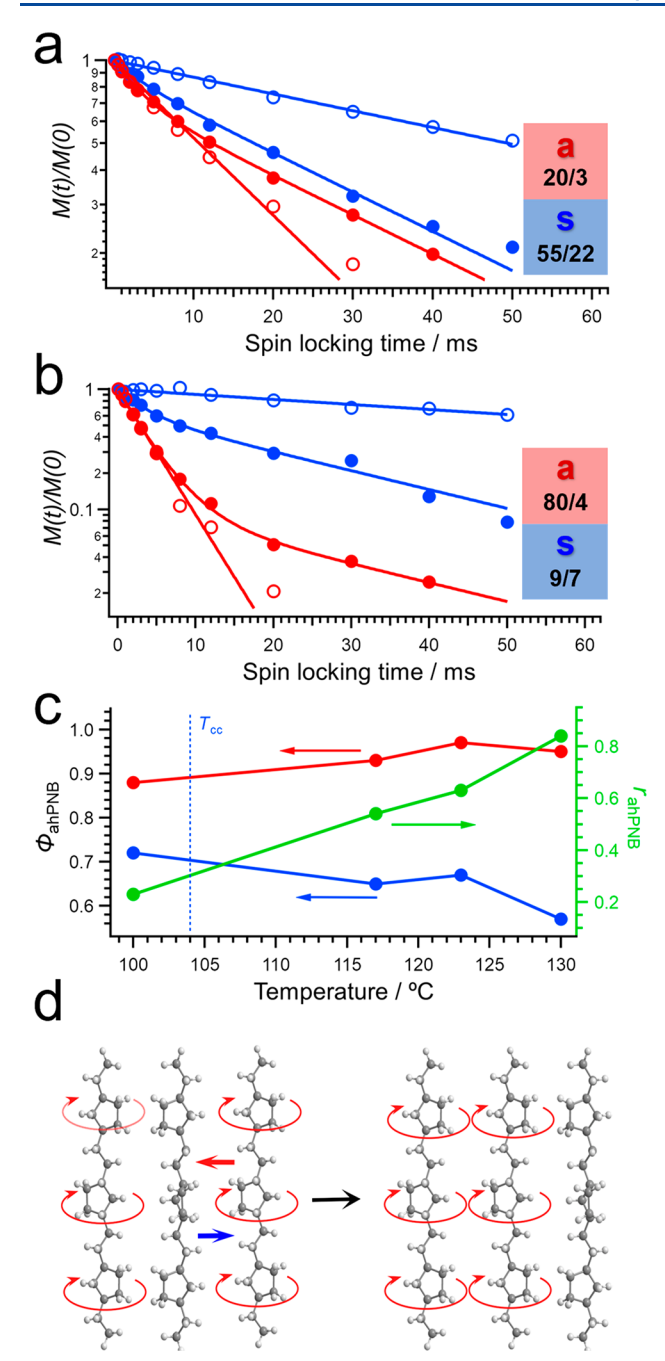


Figure 4. $T_{1\rho \rm H}$ relaxation decays for pure a- and s-hPNBs and their cocrystal at (a) 100 and (b) 130 °C. a (red) and s (blue) rectangle boxes represent a- and s-hPNB-rich domains in the heterogeneous cocrystal, with the number showing the a-/s-hPNB stem ratio in two domains determined by $T_{1\rho \rm H}$. (c) Weight fraction ($r_{\rm ahPNB}$) of a-hPNB-rich domain (green circle), and relative fraction of a-hPNB component ($\Phi_{\rm ahNB}$) in a- (red) and s-hPNB-rich (blue) domains determined by $T_{1\rho \rm H}$. (d) Schematic illustration for stem exchange dynamics for the a-/s-hPNB cocrystal.

ms, while the $T_{1\rho\rm H}$ value for pure s-hPNB increases slightly to 89.7 ms. In the blend, a- and s-hPNB relaxation curves show a large difference from those for pure components and similar curves with each other at 100 °C. This result indicates that spin diffusion occurs between a- and s-hPNB stems in the cocrystal; however, spin diffusion is not sufficient to completely average out two relaxation curves. The result implies partially spatial heterogeneity inside the cocrystal at

several nm scales. 31,32 Moreover, wide-angle X-ray diffraction (WAXD) patterns confirmed cocrystallization of a-/s-hPNBs in the blend (see Figure S3). Above T_{cO} decaying curves are further separated from each other and show obvious double-exponential behaviors. Similar relaxation curves were previously reported in the polystyrene/poly(vinyl methyl ether) blend heated above LCST. 32 Under the assumption of the (i) formation of a- and s-hPNB-rich domains, (ii) complete spin diffusion between two components within each domain, and (iii) no spin diffusion between the interdomains, the double-exponential curves were analyzed in terms of following equations: 32

$$M_a(\tau) = \chi_a^s \exp(-\tau/T_{1\rho}^s) + \chi_a^a \exp(-\tau/T_{1\rho}^a)$$
 (1)

$$M_s(\tau) = \chi_s^s \exp(-\tau/T_{1\rho}^s) + \chi_s^a \exp(-\tau/T_{1\rho}^a)$$
 (2)

where χ_a^i represents the proton molar fraction of a-hPNB in the *i* domain (*i* = *a* or *s*, $\chi_a^a + \chi_a^s = 1$), and $T_{1\rho}^i$ denotes the $T_{1\rho H}$ value of the i domain. a and s denote a- and s-hPNB-rich domains, respectively. A similar description applies to s-hPNB. The experimental curves were fitted using eqs 1 and 2. The best fit curves are shown as solid lines in Figures 4a,b and S4, and the fitting parameters are listed in Table S2. The fitting provides compositions of a- and s-hPNB-rich domains and relative fractions of two domains. Relative compositions of ahPNB stems (Φ_{ahPNB}) in a- (red circles) and s-hPNB-rich domains (blue) and relative weight fraction of a-hPNB domains $(r_{ahPNB}, green)$ as a function of temperature are plotted in Figure 4c. Weight fraction of the a-hPNB-rich domain increases with increasing temperature (green circles). Relative fraction of the a-hPNB component in the a-hPNBrich domain increases (red), while that in the s-hPNB-rich domain decreases (blue) as the temperature increases. These results indicate that nanosegregations in the cocrystal are prominent above T_{cc} .

The observed nanodomain formations can be interpreted in the following way: At around T_{co} a-hPNB stems begin large amplitude motions in a dynamic regime (>20 kHz), while shPNB stems do not. Once a-hPNB stems begin to conduct large amplitude chain dynamics, highly mobile a-hPNB and fixed s-hPNB stems give instability at the boundary between two kinds of stems. The mobile and fixed stems rearrange their locations laterally to minimize interfacial contact areas inside the cocrystals, as schematically illustrated in Figure 4d. Thermally activated a-hPNB stems can diffuse along the chain axis. Therefore, one may expect nanosegregation along the chain axis. However, individual crystalline stems are covalently bonded with the amorphous chains. The connectivity does not allow separations along the chain axis, but leads to separations into the lateral two-dimension. Therefore, the dimension of the observed phase separation in the cocrystal is different from the isotropic (three-dimensional) phase separation of the amorphous polymer blends above LCST. 25,26 Note that the lateral movement of stems occurs in the rotator phase of n-alkane. 33,34

In summary, we for the first reported asymmetric molecular dynamics and two-dimensional phase separation associated with crystal—crystal transition in the cocrystal of mobile and fixed polymer crystals. Newly obtained dynamic and spatial heterogeneities in the polymer cocrystal recall an important revision in the definition of polymer crystals that does not require "three-dimensional long-range order" but does require

"parallel packing of stems", as reported by Corradini, Auriemma, and DeRosa.³⁵

ASSOCIATED CONTENT

Supporting Information

The Supporting Information is available free of charge at https://pubs.acs.org/doi/10.1021/acsmacrolett.1c00745.

Sample preparation, DSC, WAXD and ssNMR experiments, 13 C CPMAS NMR spectra, T_{1C} and $T_{1\rho H}$ results, and WAXD patterns (PDF)

AUTHOR INFORMATION

Corresponding Authors

Toshikazu Miyoshi — School of Polymer Science and Polymer Engineering, The University of Akron, Akron, Ohio 44325-3909, United States; orcid.org/0000-0001-8344-9687; Email: miyoshi@uakron.edu

Pengju Pan — State Key Laboratory of Chemical Engineering, College of Chemical and Biological Engineering, Zhejiang University, Hangzhou 310027, China; Institute of Zhejiang University-Quzhou, Quzhou 324000, China; ◎ orcid.org/0000-0001-6924-5485; Email: panpengju@zju.edu.cn

Yuki Nakama — Zeon Corporation R&D Center, Kawasaki City, Kanagawa Prefecture 210-9507, Japan; o orcid.org/0000-0003-4997-8926; Email: y.nakama@zeon.co.jp

Authors

Ying Zheng — School of Polymer Science and Polymer Engineering, The University of Akron, Akron, Ohio 44325-3909, United States; State Key Laboratory of Chemical Engineering, College of Chemical and Biological Engineering, Zhejiang University, Hangzhou 310027, China; Institute of Zhejiang University-Quzhou, Quzhou 324000, China; orcid.org/0000-0002-2379-6342

Navin Kafle – School of Polymer Science and Polymer Engineering, The University of Akron, Akron, Ohio 44325-3909, United States

Derek Schwarz – School of Polymer Science and Polymer Engineering, The University of Akron, Akron, Ohio 44325-3909, United States

James M. Eagan — School of Polymer Science and Polymer Engineering, The University of Akron, Akron, Ohio 44325-3909, United States; ⊚ orcid.org/0000-0003-4010-9353

Shigetaka Hayano — Zeon Corporation R&D Center, Kawasaki City, Kanagawa Prefecture 210-9507, Japan; o orcid.org/0000-0001-6472-4559

Complete contact information is available at: https://pubs.acs.org/10.1021/acsmacrolett.1c00745

Author Contributions

"Y.Z. and N.K. contributed equally to this work and are co-first authors. N.Y. and S.H. synthesized samples. Y.Z., N.K., J.M.E., Y.N., P.P., and T.M. conceived and designed experiments. The manuscript was written through contributions of all authors. All authors have given approval to the final version of the manuscript.

Notes

The authors declare no competing financial interest.

ACKNOWLEDGMENTS

This work was financially supported by NSF DMR Polymers 1708999 and 2004393.

REFERENCES

- (1) Wunderlich, B.; Arakawa, T. Polyethylene Crystallized from the Melt under Elevated Pressure. *J. Polym. Sci., Part A* **1964**, *2*, 3697–3706.
- (2) Rastogi, S.; Ungar, G. Hexagonal Columnar Phase in 1,4-Trans-Polybutadiene: Morphology, Chain Extension, and IsoThermalPhase Reversal. *Macromolecules* **1992**, 25, 1445–1452.
- (3) Hikosaka, M.; Amano, K.; Rastogi, S.; Keller, A. Lamellar Thickening Growth of an Extended Chain Single Crystal of Polyethylene 1. Pointers to a New Crystallization Mechanism of Polymers. *Macromolecules* 1997, 30, 2067–2074.
- (4) Miyoshi, T.; Mamun, A. Critical Roles of Molecular Dynamics in the Superior Mechanical Properties of Isotactic-Poly(1-butene) Elucidated by Solid-State NMR. *Polym. J.* **2012**, *44*, 65–71.
- (5) Hong, Y. L.; Koga, T.; Miyoshi, T. Chain Trajectory and Crystallization Mechanisms of a Semicrystalline Polymer in Melt- and Solution-Grown Crystals as Studied using ¹³C-¹³C Double Quantum NMR. *Macromolecules* **2015**, *48*, 3282–3293.
- (6) Schulz, M.; Seidlitz, A.; Kurz, R.; Barenwald, R.; Petzold, A.; Saalwachter, K.; Thurn-Albrecht, T. The Underestimated Effect of Intracrystalline Chain Dynamics on the Morphology and Stability of Semicrystalline Polymers. *Macromolecules* **2018**, *51*, 8377–8385.
- (7) Kafle, N.; Makita, Y.; Zheng, Y.; Schwarz, D.; Kurosu, H.; Pan, P.; Eagan, J. M.; Nakama, Y.; Hayano, S.; Miyoshi, T. Roles of Conformational Flexibility in the Crystallization of Stereoirregular Polymers. *Macromolecules* **2021**, *54*, *5705*–*5718*.
- (8) Hu, W. G.; Schmidt-Rohr, K. Polymer Ultradrawability: The Critical Role of α -Relaxation Chain Mobility in the Crystallites. *ActaPolym.* **1999**, *50*, 271–285.
- (9) De Rosa, C.; Auriemma, F.; Ruiz de Ballesteros, O. A Microscopic Insight into the Deformation Behavior of Semicrystalline Polymers: The Role of Phase Transitions. *Phys. Rev. Lett.* **2006**, *96*, 167801.
- (10) Kanamoto, T.; Tsuruta, A.; Tanaka, K.; Takeda, M.; Porter, R. S. On Ultra-High Tensile Modulus by Drawing Single Crystal Mats of High Molecular Weight Polyethylene. *Polym. J.* **1983**, *15*, 327–329.
- (11) Ronca, S.; Forte, G.; Tjaden, H.; Rastogi, S. Solvent-Free Solid-State-Processed Tapes of Ultrahigh-Molecular Weight Polyethylene: Influence of Molar Mass and Molar Mass Distribution on the Tensile Properties. *Ind. Eng. Chem. Res.* **2015**, *54*, 7373–7381.
- (12) Hu, W.-G.; Boeffel, C.; Schmidt-Rohr, K. Chain Flips in Polyethylene Crystallites and Fibers Characterized by Dipolar ¹³C NMR. *Macromolecules* **1999**, 32, 1611–1619.
- (13) de Langen, M.; Prins, K. O. Mobility of Polyethylene Chains in the Orthorhombic and Hexagonal Phases Investigated by NMR. *Chem. Phys. Lett.* **1999**, 299, 195–200.
- (14) Miyoshi, T.; Mamun, A.; Hu, W. Molecular Ordering and Molecular Dynamics in Isotactic—Poly(propylene) Characterized by SS–NMR. *J. Phys. Chem. B* **2010**, *114*, 92–100.
- (15) Miyoshi, T.; Hu, W.; Li, Y. Dynamic Geometry and Kinetics of Polymer Confined in Self-Assembly via Cooperative Hydrogen Bonding: A Solid-State NMR Study under Paramagnetic Doping. *Macromolecules* **2010**, *43*, 4435–4437.
- (16) Vega, A. J.; English, A. D. Multiple-Pulse Nuclear Magnetic Resonance of Solid Polymers. Polymer Motions in Crystalline and Amorphous Poly(tetrafluoroethylene). *Macromolecules* **1980**, *13*, 1635–1647.
- (17) English, A. D. Macromolecular Dynamics in Solid Poly-(ethylene terephthalate): ¹H and ¹³C Solid-State NMR. *Macromolecules* **1984**, *17*, 2182–2192.
- (18) Hirschinger, J.; Miura, H.; Gardner, K. H.; English, A. D. Segmental Dynamics in the Crystalline Phase of Nylon 66: Solid State Deuterium NMR. *Macromolecules* **1990**, 23, 2153–2169.
- (19) Wittmann, J. C.; Smith, P. Highly Oriented Thin Films of Poly(tetrafluoroethylene) as a Substrate for Oriented Growth of Materials. *Nature* **1991**, 352, 414–417.
- (20) Utracki, L. A. Polymer Alloys and Blends: Thermodynamics and Rheology; Hanser Pub. Inc., 1990.

- (21) Lodge, T. P.; Mcleish, T. C. B. Self-Concentration and Effective Glass Transition Temperatures in Polymer Blends. Macromolecules 2000, 33, 5278-5284.
- (22) Chung, G.-C.; Kornfield, J. A.; Smith, S. D. Component Dynamics in Miscible Polymer Blends: A Two-Dimensional Deuteron NMR Investigation. Macromolecules 1994, 27, 964-973.
- (23) Roland, C. M.; Casalini, R. The Role of Density and Temperature in the Dynamics of Polymer Blends. Macromolecules **2005**, 38, 8729-8733.
- (24) Gill, L.; Damron, J.; Wachowicz, M.; White, J. L. Glass Transitions, Segmental Dynamics, and Friction Coefficients for Individual Polymers in Multicomponent Polymer Systems by Chain-Level Experiments. Macromolecules 2010, 43, 3903-3910.
- (25) Kwei, T. K.; Nishi, T.; Roberts, R. F. A Study of Compatible Polymer Mixtures. Macromolecules 1974, 7, 667-674.
- (26) Tanaka, H. Universality of Viscoelastic Phase Separation in Dynamically Asymmetric Fluid Mixtures. Phys. Rev. Lett. 1996, 76, 787-790.
- (27) Hayano, S.; Nakama, Y. Iso- and Syndio-Selective ROMP of Norbornene and Tetracyclododecene: Effects of Tacticity Control on the Hydrogenated Ring-Opened Poly(cycloolefin)s. Macromolecules **2014**, *47*, 7797–7811.
- (28) Lee, L.-B. W.; Register, R. A. Hydrogenated Ring-Opened Polynorbornene: A Highly Crystalline Atactic Polymer. Macromolecules 2005, 38, 1216-1222.
- (29) Nakama, Y.; Hayano, S.; Tashiro, K. Influence of Tacticity on the Crystal Structures of Hydrogenated Ring-Opened Poly-(norbornene)s. Macromolecules 2021, 54 (17), 8122-8134.
- (30) Liu, S. F.; Mao, J. D.; Schmidt-Rohr, K. A Robust Technique for Two-Dimensional Separation of Undistorted Chemical-Shift Anisotropy Powder Patterns in Magic-Angle-Spinning NMR. J. Magn. Reson. 2002, 155, 15-28.
- (31) Mirau, P. A Practical Guide to Understanding the NMR of Polymers; John Wiley & Sons, Inc., 2005.
- (32) Asano, A.; Takegoshi, K.; Hikichi, K. ¹³C c.p./m.a.s. n.m.r, Study on the Miscibility and Phase Separation of a Polystyrene/ Poly(vinyl methyl ether) Blend. Polymer 1994, 35, 5630-5636.
- (33) Yamakawa, H.; Matsukawa, S.; Kurosu, H.; Kuroki, S.; Ando, I. Diffusional Behavior of n Alkanes in the Rotator Phase as Studied by Pulse Filed-Gradient Spin-Echo ¹H NMR Method. J. Chem. Phys. **1999**, 111, 7110-7115.
- (34) Yamamoto, T. Molecular Dynamics of Crystallization in n-Alkane Mixtures; Texture, Compatibility, and Diffusion in Crystals. Polymer 2016, 99, 721-733.
- (35) Corradini, P.; Auriemma, F.; De Rosa, C. Crystals and Crystallinity in Polymeric Materials. Acc. Chem. Res. 2006, 39, 314-

□ Recommended by ACS

Crystallization of Propene-Pentene Isotactic Copolymers as an Indicator of the General View of the Crystallization Behavior of Isotactic Polypropylene

Miriam Scoti, Claudio De Rosa, et al.

DECEMBER 23, 2021 MACROMOLECULES

Minimum Molecular Weight and Tie Molecule Content for Ductility in Polyethylenes of Varying Crystallinity

Seong Hyuk Cho and Richard A. Register

APRIL 13, 2022

MACROMOLECULES

READ **C**

Chain-End Modification: A Starting Point for Controlling Polymer Crystal Nucleation

Kyle Wm. Hall, Michael L. Klein, et al.

FEBRUARY 02, 2021

MACROMOLECULES

RFAD 17

Tammann Analysis of the Molecular Weight Selection of Polymorphic Crystal Nucleation in Symmetric Racemic Poly(lactic acid) Blends

Yucheng He, Wenbing Hu, et al.

APRIL 14, 2022

MACROMOLECULES

RFAD 🗹

Get More Suggestions >